

Southwest Pacific atmospheric weather regimes: linkages to ENSO and extra-tropical teleconnections

Andrew M. Lorrey^{a*}  and Nicolas C. Fauchereau^b

^a National Institute of Water and Atmospheric Research, Auckland, New Zealand

^b National Institute of Water and Atmospheric Research, Hamilton, New Zealand

ABSTRACT: We objectively identified an optimal number of atmospheric weather regimes, also called synoptic types, within the southwest (SW) Pacific tropical–subtropical domain and examined their potential drivers. Six atmospheric weather regimes in this region are characterized by spatially heterogeneous geopotential height, sea surface temperature, and regional precipitation patterns. The identified weather regimes are phase-locked to the seasonal cycle with a moderate degree of coherency, and some are capable of persisting for weeks or more in extreme cases. Correlations between the SW Pacific weather regimes and global precipitation reanalysis fields indicate a strong connection between regional weather patterns and South Pacific convergence zone (SPCZ) mean position changes and relative intensity of convective loci within the SPCZ. Climate field correlations to SW Pacific weather regimes also show distinct geopotential height and SST signatures across Southern Hemisphere middle and high latitudes and the Indian Ocean basin. Strong statistical significance for portions of those spatial patterns lends support to the assertion of extra-basin teleconnections for SW Pacific weather regimes. There are strong precipitation impacts from SW Pacific weather regime frequency changes and regime persistence on extreme rainfall deficits and/or surpluses for small islands during austral summer. Diagnostic analysis of the spatial correlation fields and each weather regime indicates these weather patterns are connected to eastern equatorial Pacific-styles of El Niño and La Niña and Modoki La Niña. Another regime type appears to be connected to an enhancement of the Hadley–Ferrell circulation, while two other types are influenced by phenomena that arise outside the Pacific basin (Madden–Julian oscillation, Southern Annular Mode, and Pacific South American mode). SW Pacific weather regime investigations in the context of modern climate, palaeoclimatology, and future climate change scenarios can help to surmount spatial-scale mismatches that exist between global models and small Pacific islands, while helping to improve general understanding of island-scale impacts from atmospheric circulation.

KEY WORDS synoptic types; ENSO; Pacific Islands; rainfall; reanalysis fields

Received 7 July 2016; Revised 3 August 2017; Accepted 4 September 2017

1. Introduction

Previous work has shown regional-scale daily weather patterns that characterize the near-surface atmospheric circulation (i.e. synoptic circulation) can be decomposed into discrete and recurrent archetypes called ‘atmospheric circulation regimes’ or ‘weather regimes’ (WR thereafter). WRs are an important paradigm for extra-tropical weather and climate research because they can be interpreted as dynamical attractor basins in phase space that is visited by atmospheric circulation (Mo and Ghil, 1988; Vautard and Legras, 1988; Kimoto, 1989; Vautard, 1990).

Synoptic weather typing has been successful in the Northern Hemisphere (NH), where multiple studies have applied a range of clustering algorithms to daily atmospheric circulation data sets as a way to derive regionally prominent WRs (Mo and Ghil, 1988; Vautard, 1990;

Michelangeli *et al.*, 1995; Cassou, 2008). In many cases, WRs correspond to large-scale climate modes (i.e. North Atlantic oscillation; NAO+, NAO– phases) and other regionally specific geographic patterns (i.e. ‘Atlantic Ridge’ WR and a ‘Scandinavian Blocking’ WR), which can influence their frequency of occurrence.

Regional climate anomalies (e.g. temperature and rainfall) in Europe are demonstrated to arise from changes in the occupation statistics of WRs that are modulated by large-scale climate modes that operate at intra-seasonal to inter-annual time scales (e.g. Yiou and Nogaj, 2004). As such, the prediction potential of hydroclimatic impacts beyond weather time scales (Baldwin and Dunkerton, 2001) can be enabled by a better understanding of WR behaviour.

Elsewhere, linkages between daily meteorological conditions from WRs and seasonal-to-intra-seasonal variability show connections to climate phenomenon such as the monsoon (Qian *et al.*, 2012), Madden–Julian oscillation (MJO; Cassou, 2008; Fauchereau *et al.*, 2016) and El Niño–Southern Oscillation activity (ENSO; Moron and Plaut, 2003; Moron *et al.*, 2016). However, with respect

*Correspondence to: A. M. Lorrey, National Centre for Climate, Atmosphere and Hazards, National Institute of Water and Atmospheric Research, 41 Market Place, Viaduct Precinct, Central Business District, Auckland 1010, New Zealand. E-mail: a.lorrey@niwa.co.nz

to NH continental regions, WR research has been less applied in the Tropics than in the extra-tropics. Because tropical circulation is dominated by convective activity and boundary forcings (e.g. sea surface temperature anomalies, SSTa) that are inherently more important than in the extra-tropics, the dynamical interpretation of WRs is less clear than in extra-tropical circulation situations.

While there is limited application of WR work for the SW Pacific or the Tropics elsewhere (Kidson, 2000; Lefèvre *et al.*, 2010; Ackerley *et al.*, 2011; Renwick, 2011; Jiang *et al.*, 2013; Moron *et al.*, 2016), the studies that do exist demonstrate they can critically improve understanding of climate driver impacts, including those from ENSO. The spatial displacement and changes in convection for the inter-tropical convergence zone (ITCZ) and South Pacific convergence zone (SPCZ; Matthews, 2012; Widlansky *et al.*, 2011) during ENSO events, for example, have notable effects on Pacific Island rainfall. They also can influence regional patterns of tropical cyclone occurrence (Diamond *et al.*, 2013) and extra-tropical transition of tropical cyclones (Lorrey *et al.*, 2014b) that can impact the lives of millions of people. As such, there is a significant impetus to better understand WRs in the SW Pacific.

In this paper, we undertake a synoptic weather typing exercise that is applied to the southwest Pacific basin (10°N – 30°S , 160°E – 130°W ; see Section 3.1 for test of domain results). The inevitable choice of domain was motivated by the importance of the SW Pacific in the global climate system and by the large degree of regional climate variability – and associated detrimental impacts – that affect the Pacific Islands (e.g. drought, deluge, and tropical cyclones; Lorrey and Renwick, 2011; Diamond *et al.*, 2013). We expect that a WR view of atmospheric circulation variability in the SW Pacific will contextualize interpretations of past weather and climate events and improve prediction of regional and local impacts of atmospheric circulation regimes from weather to seasonal time scales.

2. Methods

2.1. Data

2.1.1. Climate fields

We determined South Pacific (SP) WRs using daily geopotential heights from NCEP/NCAR1 (Kalnay *et al.*, 1996) over the period spanning the 1 January 1950 to 31 December 2014 (29 February removed on leap years). Monthly averages of the zonal (U) and meridional (V) components of 850 and 200 hPa were also obtained for analysis (<http://www.esrl.noaa.gov/psd/data/gridded/data.ncep.reanalysis.html>). Monthly sea surface temperatures were derived from the ERSSTv3b data set, available over the 1948–2014 period at a monthly time resolution and over a 2×2 degree grid (downloaded from <ftp://ftp.ncdc.noaa.gov/pub/data/cmb/ersst/v4/netcdf>).

Monthly rainfall anomalies were also calculated from the Global Precipitation Climatology Project (GPCP) data set (version 2; Adler *et al.*, 2003) which merges data from rain

gauge stations, satellites, and sounding observations on a 2.5° global grid from 1979 to the present. For all spatial data drawn from these reanalysis data sets, the long-term (linear) trend was removed prior to further analysis. All monthly anomalies were calculated with respect to the 1981–2010 climatology to be consistent with the treatment of the other data sets and indices.

2.1.2. Climate indices

The coupled ENSO index (CEI) was initially developed by Gergis and Fowler (2005) as a way to indicate the relative strength and alignment of key atmospheric and oceanic indicators of ENSO. We have adopted that style of classification and recalculated the CEI over the period 1950–2014 from the original Southern Oscillation Index (SOI) and Niño3.4 values, with anomalies calculated with respect to the 1981–2010 climatology.

The SOI is first calculated from the raw mean sea level pressure (MSLP) data for Tahiti (T) and Darwin (D) made available online by the Australian Bureau of Meteorology (BoM) at <ftp://ftp.bom.gov.au/anon/home/ncc/www/sco/soi>. The SOI is calculated following the Troup (Troup, 1965) method as:

$$\text{SOI} = [(T - T_{\text{c}}) - (D - D_{\text{c}})] / [\text{SD} (T - D)] \quad (1)$$

The 1981–2010 climatological averages for Tahiti (T_{c}) and Darwin (D_{c}) surface pressures and SD is the standard deviation of the MSLP difference between these two locations.

The CEI uses the Niño3.4 temperature anomalies in the central western equatorial Pacific (5°S – 5°N , 120°W – 170°W) for its oceanic component. The monthly Niño3.4 sea surface temperatures index from the ERSSTv3b data set were used, and are made available by the Climate Prediction Center at <http://www.cpc.ncep.noaa.gov/data/indices/ersst3b.N<math>\text{N}</math>.ascii>.

Running averages (3 months for the SOI, 5 months for the Niño3.4 index) are then calculated, the CEI being defined as:

$$\text{CEI} = (\text{SOI}^* - 1) + \text{Niño3.4} \quad (2)$$

The CEI categories are defined according to simultaneous values of the SOI and the Niño3.4, whereby if both the SOI and Niño3.4 exceed set thresholds for El Niño (La Niña), it is termed a CEI Niño (Niña) event. Likewise, an ocean-dominated event is indicated when only the Niño3.4 index exceed the threshold, and similarly for atmospheric-dominated event. The oceanic thresholds used for Niño3.4 are $\pm 0.5^{\circ}\text{C}$ for the 5-month mean and the SOI threshold is ± 1 SD for the 3-month mean. A previous classification of ENSO events using the CEI and comparison to other ENSO classification schemes are found in Gergis and Fowler (2005).

It has been recognized over the past decades that there are more than three simple states of ENSO (positive,

neutral, and negative). Leading paradigms indicate there is a continuum of ENSO composed of different typologies (Capotondi *et al.*, 2015), with ENSO phases occurring in more than one ‘flavour’ that have main distinctions related to the longitude of the maximum SST anomalies along the Equator (Johnson, 2013). For the latter perspective, ‘canonical’ ENSO flavours can have SST spatial anomalies that are strongly centred in the far eastern and far western equatorial Pacific, while a more recently recognized ENSO variation shows core anomalies for the ‘eastern pole’ that are centred closer to the International Date Line. This latter type of ENSO has been referred to in the literature as the ‘dateline El Niño’ (Larkin and Harrison, 2005), ‘El Niño Modoki’ (Ashok *et al.*, 2007), ‘warm pool El Niño’ (Kug *et al.*, 2009), and ‘central Pacific El Niño’ (Yeh *et al.*, 2009). We use a measure of ENSO called the El Niño ‘Modoki’ index (EMI) that has been calculated from the ERSST SST anomalies (1981–2010 climatological normal) by Ashok *et al.* (2007) as:

$$\text{EMI} = (\text{SSTA}) A - 0.5^* (\text{SSTA}) B - 0.5^* (\text{SSTA}) C \quad (3)$$

SSTA represents the ‘area-averaged SST anomalies’ over segments of the central Equatorial Pacific, divided into subregions *A* (165°E – 140°W , 10°S – 10°N), *B* (110°W – 70°W , 15°S – 5°N), and *C* (125°E – 145°E , 10°S – 20°N), respectively. We further divide the EMI in three categories: ‘EMI+’, ‘EMI−’, and ‘Neutral’, using ± 1 SD as thresholds.

We focus on the two aforementioned indices and use them to assess the sensitivity of WR frequency with regard to the co-occurring ocean–atmosphere conditions for ENSO events (as seen through the CEI) as well as the ‘flavour’ of ENSO (‘canonical’ or eastern Pacific type of ENSO vs ‘Modoki’ or central Pacific type of ENSO) via the EMI.

2.1.3. Station rainfall data

Historic monthly rainfall returns from the Pacific Islands Meteorological Services that are held in the New Zealand National Institute of Water and Atmospheric Research (NIWA) climate database are utilized. High-quality stations with less than 2% missing monthly data for 1950–2014 were selected from that database, and rainfall totals (in mm) and percent rainfall anomalies relative to the 1981–2010 climatology interval were calculated. The December–February monthly mean anomalies were then averaged together to produce mean austral summer seasonal anomaly values. All seasonal mean calculations were required to have at least two of the 3-month totals present (or else they were omitted).

2.2. Analyses

2.2.1. Cluster analysis: test of domain area and spatial field

Daily anomalies of geopotential height at 1000, 850, 500, and 200 hPa (z_{1000} , z_{850} , z_{500} , and z_{200}) for several discrete areas of the SP domain were evaluated with respect

to the 1981–2010 climatic normal period. These anomalies were subjected to empirical orthogonal function (EOF) decomposition, and the first eight principal components (PCs), which explained up to 80% of the original variance, were retained to form the reduced space within which the clustering procedures were applied.

One of the caveats of most clustering algorithms is that *a priori* assignment of the number of clusters (*K*) must be made. However, it is usually unclear what the ‘optimal’ number of clusters is for climate data sets. Recently, the so-called affinity propagation (AP) algorithm has been introduced (Frey and Dueck, 2007). The AP algorithm is based on the concept of ‘message passing’ between data points and uses the dissimilarity matrix as an input. Unlike clustering algorithms such as k-means or k-medoids (Kaufman and Rousseeuw, 1990; Park and Jun, 2009) AP does not require the number of clusters to be determined *a priori*. Like k-medoids, AP finds ‘exemplars’; these are members of the input set that are representative of clusters, and the AP assigns each point in the given data set to the closest exemplar.

A drawback of this algorithm is its complexity and associated computing requirements. AP has a time complexity of the order $O^*(N^2*T)$, where *N* is the number of samples and *T* is the number of iterations until convergence. Furthermore, the memory complexity is of the order $O^*(N^2)$. In the present study *N* = 23 725 days (daily data over the 1 January 1950 to 31 December 2014 period), which makes using AP directly for determination of the WRs prohibitive. We therefore adopted a Monte-Carlo approach to determine the optimal partition (optimal number of WRs): we applied AP repeatedly (*P* = 1000) on samples (size *N* = 2000) drawn from the original data set (i.e. the base formed by the aforementioned eight PCs). Any natural partition of this data set should emerge as a peak in the distribution of *K* among the *P* iterations. Once the latter is determined, the standard – and computationally efficient – *k*-means clustering algorithm (Hartigan, 1975; Michelangeli *et al.*, 1995) can then be applied to yield the set of WRs.

2.2.2. Relationship to climate modes

In accord with previous work (Moron and Plaut, 2003; Cassou, 2008; Riddle *et al.*, 2013; Moron *et al.*, 2016), we investigated how the occupation statistics (i.e. the probability of occurrence) of SP WRs are modulated by large-scale, slow varying climate modes. Our main focus was ENSO, with a particular interest on the relationships of each WR to different styles of co-occurring ocean – atmosphere conditions for ENSO events. Because of the phase-locking of ENSO to the annual cycle (Tziperman *et al.*, 1994) and the presence of a seasonal component in the distribution of the WR (Figure 3), there is a need to account for both the phase of ENSO and the time of the year with regard to WR frequency. We applied overlapping 3-month window (i.e. DJF, JFM, etc.) calculations of each WR frequency and attributed the calculated statistics (e.g. probability of occurrence of the WRs or transition

probabilities) to the middle month (e.g. January indicates the value for DJF) when plotted through time.

2.2.3. Significance of the occupation statistics changes for WRs

From a statistical standpoint, the time sequence of WR occurrence can be summarized by the number of days each WR is observed over the period considered, which also is used to show probabilities of transitioning from one WR to the next. The WR transition probabilities include persistence (probability of ‘staying’ in the same WR). This perspective closely corresponds to the definition of a discrete time Markov chain (DTMC; Wilks, 2011).

The information that is encapsulated by WR probabilities and transition matrices lend to DTMC being employed as the basis of a Monte-Carlo significance test. This test requires generation of an arbitrary number of time series of the discrete WRs of any length, whose statistical properties are virtually identical to the observed time series (when long periods are considered). Our application of this tactic is essentially similar to the methodology exposed in Riddle *et al.* (2013), Lorrey *et al.* (2014a), and Fauchereau *et al.* (2016). Specifically, and using an example with the CEI, 10 000 artificial time series of WRs occurrences were performed independently for each season (DJF, JFM, etc.) and CEI phase (seven categories, Section 2.1). The change in probability (compared to the observed climatological occurrences) of observing a given WR is then calculated for each of the 10 000 synthetic realizations. The 95% confidence limit is drawn from this null distribution, so that the observed anomaly in the frequency of a WR is considered significant at the 95% confidence level if it is below the corresponding simulated 5th percentile for negative anomalies (above the 95th percentile for positive anomalies).

3. Results

3.1. Cluster analysis test of domain area and spatial field

The WR domain was considered for a discrete spatial area that would adequately capture variations in both the position and intensity of the SPCZ. Our reasoning for this choice is because the SPCZ has prominent influences on Pacific Island rainfall on inter-seasonal time scales. There are strong connections between the SPCZ and ENSO (Vincent *et al.*, 2011), which have direct impacts on regional sea surface temperatures and overlying atmospheric circulation properties. The SPCZ region of definition has previously been ascribed by Widlansky *et al.* (2011), and it extends from Papua New Guinea to French Polynesia. In essence, the choice of including larger or smaller areas around the core SPCZ zone are somewhat arbitrary, but whatever WRs can be defined should remain relatively insensitive to a subtle shifts in the domain size and location. As such, we tested four different spatial domains [1: (-40, 0, 140, 230), 2: (-40, 0, 160, 230), 3: (-30, 10, 150, 220), 4: (-30, 10, 160, 230)] that included the core area of SPCZ activity and also the equatorial region of ENSO SST activity (Figure S1 in Appendix S1,

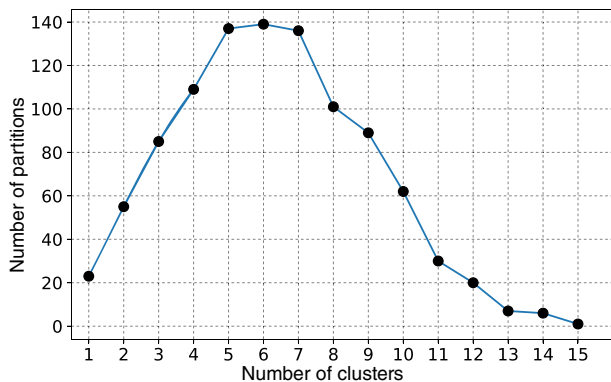


Figure 1. Distribution of the number of partitions for a given K (number of clusters) as determined by repeated AP for the SW Pacific region based on detrended NCEP1 geopotential at 1000 hPa, 1950–2014. [Colour figure can be viewed at wileyonlinelibrary.com].

Supporting information) prior to undertaking a full suite of in depth analyses. We also evaluated whether discrete WR archetypes at different atmospheric levels achieved different optimal values.

The results of that antecedent evaluation indicated that z1000 leads to the most compact representation of daily atmospheric circulation across all of our selected spatial domains, with the optimal number of WR clusters increasing with altitude through the atmosphere. As such, z1000 was used for further assessment on the sensitivity of domain spatial choice. The distribution of K s as determined by AP for the 1000 iterations (Section 2.1) indicated the optimal number of WRs is between three and nine, with a local peak of six types (Figure 1). The computationally efficient k -means clustering algorithm was then applied specifying $K = 6$, for the four different test spatial domains. When we cross-correlated the resultant spatial field patterns for each WR cluster according to the chosen spatial domain (1–3 = test domains, 4 = control domain), each of the six discrete WRs were found for every southwest Pacific domain choice, regardless of whether the analysis domain was shifted south and east by 10° or even expanded either south or westwards (even by up to 20° of longitude). As such, we used the results of z1000 for domain 4 ($-30, 10, 160, 230$) to ascribe regional WRs for the SW Pacific, and the domain choice closely follows a region circumscribing the SPCZ (Widlansky *et al.*, 2011). The composite daily z1000 geopotential anomalies (relative to 1981–2010 climatic normal base period) for each of the six WRs, as well as the number of days they are observed show the main spatial characteristics of regional atmospheric circulation and the resultant near-surface wind field patterns (Figure 2).

As in previous WR studies (Kidson, 2000), the spatial locations of geopotential height anomalies in the domain can be used to describe each regime and the circulation across the area of interest. We provide preliminary descriptors for each of these regimes here, but continue to refer to them in the text in their numeric format. A majority of the regimes contain low-pressure anomalies that are situated in different locations, on average, within the chosen

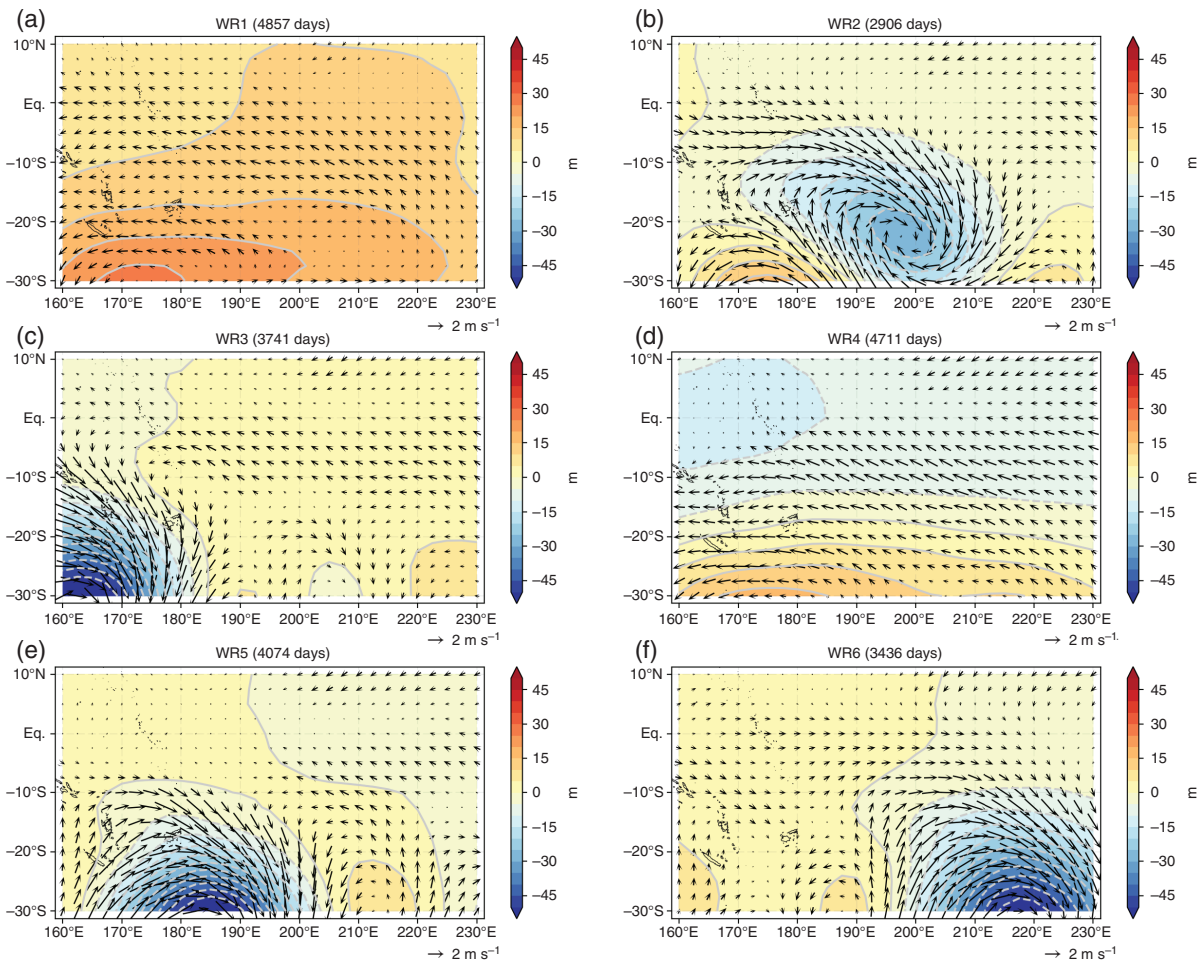


Figure 2. $z1000$ Geopotential composite anomalies (in m) for all days attributed to each of the six SP clusters (regimes). The number in parenthesis indicates the occurrence for each regime (days) drawn from the reanalysis. Short descriptors of the atmospheric circulation associated with each weather type are as follows: WR1 – high over South Pacific, HSP; WR2 – subtropical low, STL; WR3 – trough in the north Tasman, TNT; WR4 – enhanced climatological pattern, EC; WR5 – trough northeast of New Zealand, TNZ; WR6 – trough over French Polynesia, TFP. Grey arrows show vector winds.

domain. WR1 has a distinct high-pressure anomaly over the SW Pacific (hence named ‘HSP’ type), WR2 has a moderately strong low pressure centre to the east of the International Date Line in the subtropics (subtropical low or ‘STL’ type), and a high-pressure anomaly to the southwest of it in the north Tasman Sea, lending to enhanced westerly-to-northerly quarter flow across many islands. WR3 sees more frequent troughs in the north Tasman Sea (‘TNT’ type) and an associated wind flow pattern across the domain that is largely opposite of WR6, which has a deep low (trough) over French Polynesia (‘TFP’ type). WR4 shows spatial traits that are essentially an amplification of equatorial low-pressure and mid-latitude high-pressure belts (enhanced climatological pattern or ‘EC’ type). WR5 shows a strong trough to the northeast of New Zealand (‘TNZ’ type) and a high-pressure anomaly south of the Austral Islands that produces stronger meridional flow across many SW Pacific islands.

3.2. WR climatological properties

While the seasonal cycle and long-term trend have been removed from the daily $z1000$ time series prior to the

clustering procedure, the distribution of most WRs presents some degree of seasonality. For the climatology (1981–2010) of WR occurrence on a 3-monthly basis (Figure 3, plotted by central month), WR5 and WR6 occur more frequently during the austral cool and dry season (May–October). WR2 tends to occur more frequently during the austral summer season (December–February) while WR3 sees a gradual increase in frequency from austral summer through the following austral spring. WR2 has the strongest amplitude in terms of frequency change over the course of a year, while WR1 has the lowest amplitude for changes in frequency, occurring almost uniformly throughout the year.

3.3. Persistence and transitions

The distribution of WR sequence length (number of consecutive days a WR is observed), the transition probabilities (i.e. difference between the observed transition probabilities and what would be expected given the overall frequency of the WRs), and prevalence of self-transitions across the annual cycle were calculated for all seasons over

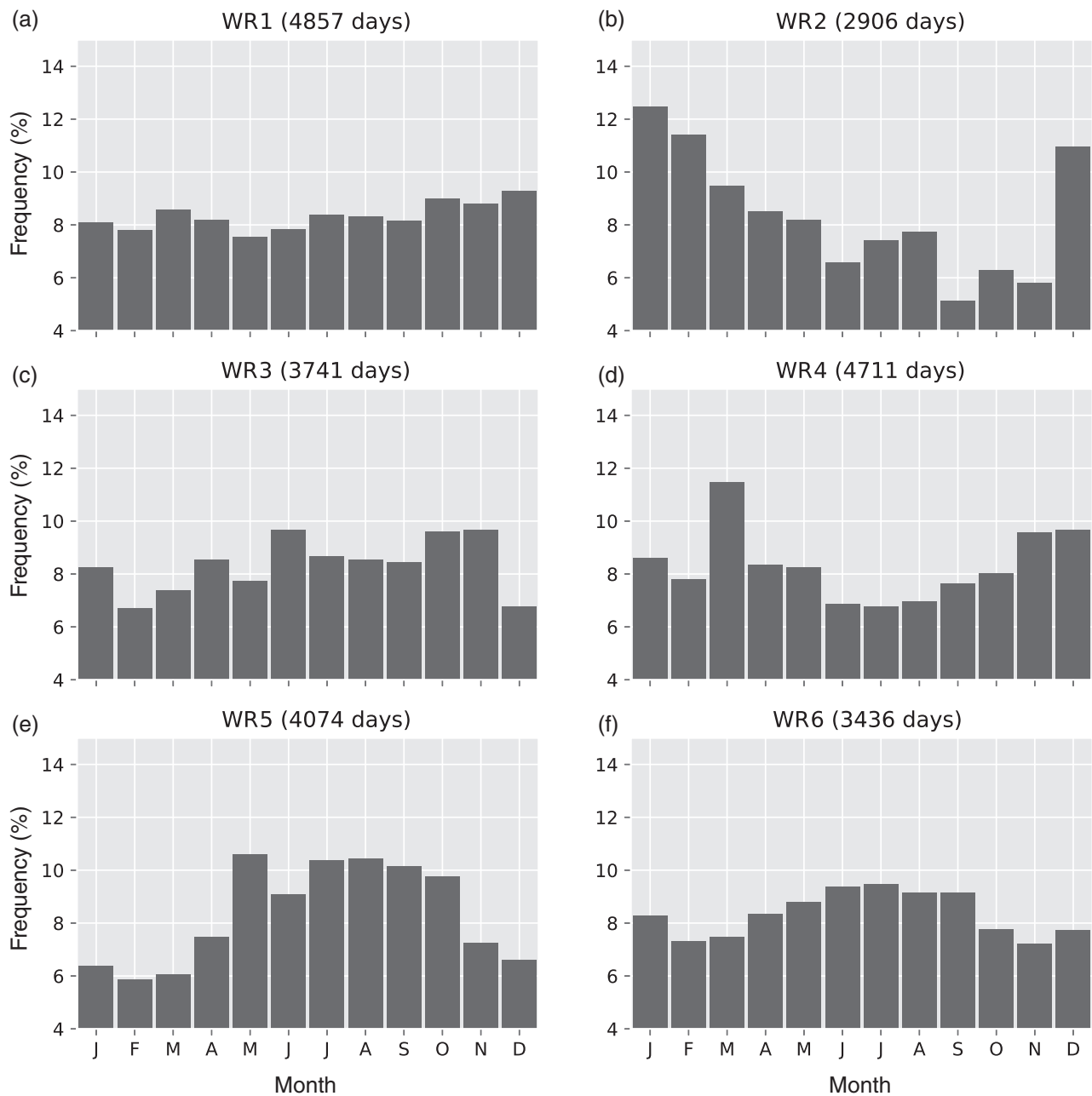


Figure 3. Monthly frequency changes for six southwest Pacific atmospheric WRs, showing the percentage of the total number of days within each month they occur.

the 1981–2010 period (Figures 4(a)–(c)). WR persistence metrics are summarized in Figure 4.

The distribution of the consecutive sequence length is positively skewed for all WRs. Most of the regimes last 2 or 3 days, and rare occurrences of SP WR sequences can last multiple weeks (Figure 4). WR4 is the most persistent regime on average (~ 3.3 days) and has a moderately long maximum sequence length (20 days). WR1 and WR6 have the longest maximum observed persistence (26 days) compared to the other WRs (Figure 4(a)). The longest consecutive sequence is observed for WR1 and WR6, with one WR1 sequence lasting 26 consecutive days from 25 January 2011 to 19 February 2011 and one for WR6 that lasted from 10 January to 4 February 1998.

Figure 4(b) presents the observed transitions from one WR to another, expressed as deviations of their expected probability relative to the overall frequency of each WR occurrence in the observed record. For example, the transition from WR3 to WR5 is 83.5% more frequent than what could be expected by chance only given the frequency of WR5 in the period of observation. Some preferred transition paths are evident (e.g. the sequence WR2–WR6 and WR3–WR5 are more frequent than what could be expected by chance). On the other hand, some transitions and transition paths are ‘highly unlikely’ (far less frequent than what one could expect by chance). Examples of this are the transition WR3–WR4 and WR2–WR4, both at least 40% less frequent than what could be expected

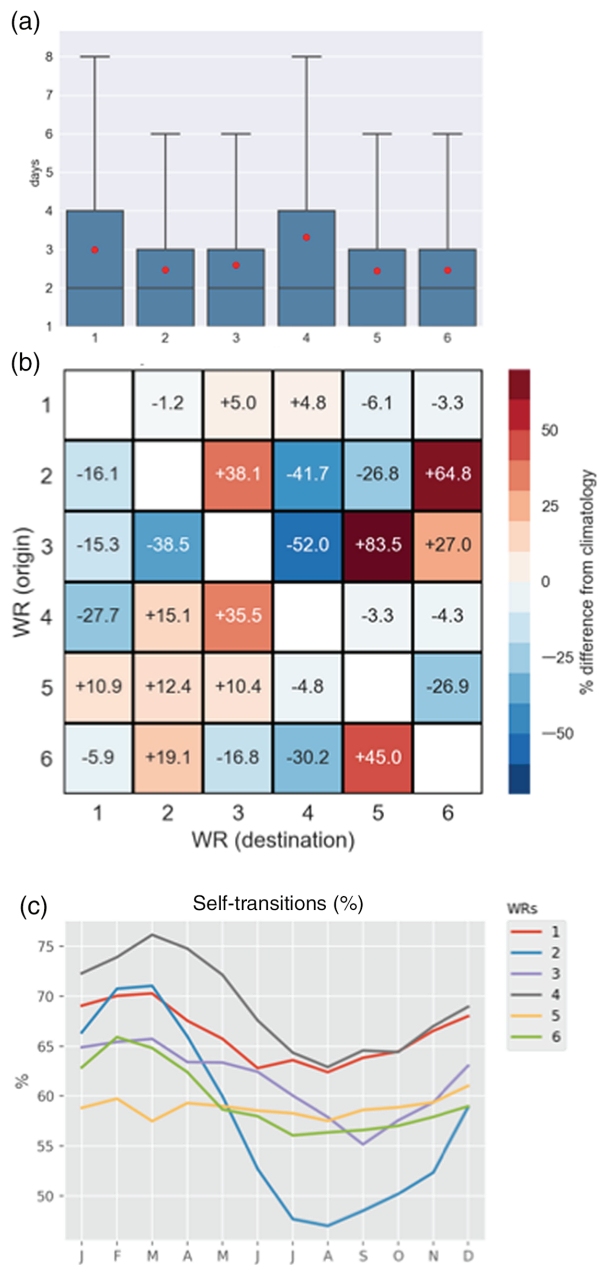


Figure 4. SW Pacific atmospheric WR persistence and WR transitions. (a) The blue boxes for the WR persistence span the 25th–75th percentile, the horizontal black line is the median persistence for each regime, the dot is the mean and the whisker is the 95th percentile. (b) The WR transitions are expressed as percentage changes with respect to what should be expected by chance if only given the overall frequency of each WR. The transitions are read from row to column; that is, +83.5% is the percentage difference (from expected probability given the frequency of WR5) to transition from WR3 to WR5. (c) Annual climatology of WR transitions showing the percentage of time in any month for a regime to transition to itself.

by chance. While beyond the scope of this particular study, these preferred or unlikely transition paths have implications in terms of predictability at the sub-seasonal time scale.

For most of the WRs that have been identified in this study, there is a higher prevalence of self-transition (i.e. persistence) during the months of the year (February and

March) when tropical SSTs are at their highest (and conversely when persistence is lowest). The exception to this is seen for WR5, which has a relatively stable degree of self-transition through the year (Figure 4(c)).

3.4. Relationships to the large-scale climate background state

The relationships between inter-annual variability of SP WRs and large-scale climate conditions are assessed using the correlation fields for monthly WR frequency anomalies *versus* monthly SSTa (Figure 5) and 850 hPa geopotential anomalies (z850; Figure 6).

Overall, SSTa (Figure 5) and z850 (Figure 6) spatial correlations for three of the WR (1, 3, 6) are configured in an arrangement reminiscent of ocean and atmosphere patterns typically associated with ENSO. WR1 and WR3 have correlation patterns that are akin to the spatial expression of two types of La Niña (Song *et al.*, 2016). WR1 has SSTa correlations along the Equator that are strongest to the east of the International Date Line. WR3 has correlations to SST along the Equator that appear strongest west of the International Date Line along with much stronger subtropical and extra-tropical SST correlations than WR1. WR3 and WR6 have largely opposite geopotential correlation signatures from the Tropics to the high southern latitudes, which (along with other metrics) suggest they represent opposite ENSO phases (see Section 3.5 for further explanation). WR1 has spatial correlations for SSTs that appear similar to the ENSO-like SST correlations for WR3 but the correlation field pattern appears weaker across the Pacific, and the distribution of the positive and negative correlations outside of the Pacific basin also appear different from WR3. In addition, the spatial correlation pattern seen in the z850 field for WR1 does not look like what is observed for WR3 (or its counterpart WR6; Figure 6), which has a more typical atmospheric mass ‘see-saw’ pattern for northern Australia/Maritime Continent and French Polynesia, potentially in conjunction with a pattern similar to what may be observed for the Pacific South American (PSA) mode. Overall, the strongest SST correlations (Figure 5) for all six WRs are found in the central and subtropical Pacific basin, while weaker correlations (for most regimes, except WR1, WR3, WR6, and weakly for WR5) are observed in the higher latitudes and in the Indian Ocean basin.

While SST correlations appear weak and inconsistent for WR2, WR4, and WR5 (Figures 5(b), (d), and (e), respectively), their z850 spatial correlations (Figures 6(b), (d), and (e)) have strong signatures. WR4 has a z850 correlation pattern that is similar to the climatological expression of an enhanced Hadley–Ferrell cell circulation. The strongest negative correlations for that regime are orientated in a zonal pattern along the equator (akin to the region of low pressure where the Hadley circulation rises) and are accompanied by positive correlations along the middle latitudes of both hemispheres in the locations where the Hadley and Ferrell cells descend to generate a high-pressure belt.

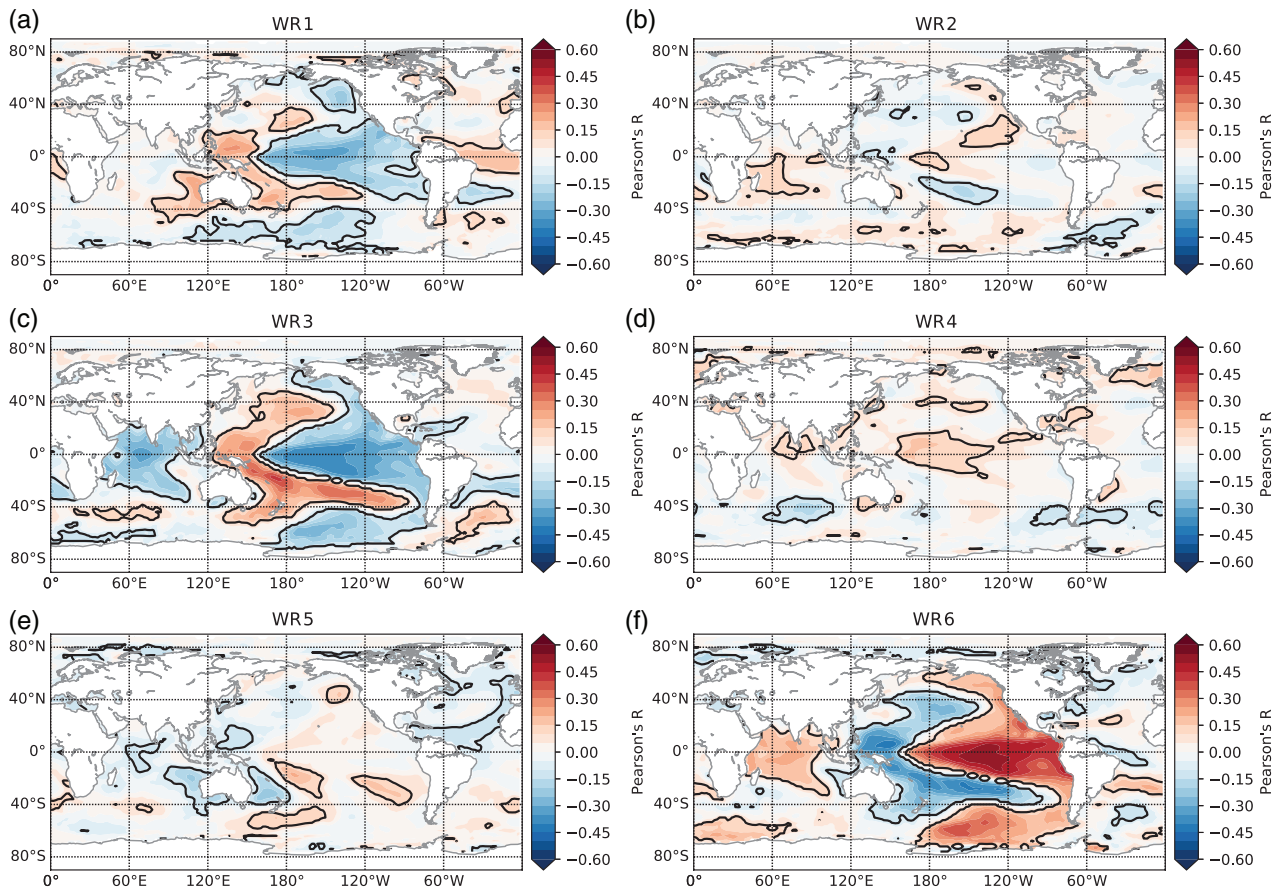


Figure 5. Correlation between SW Pacific atmospheric WR frequency (1950–2014) and global monthly SST anomalies (based on ERSSTv4). The climatological period for the calculation of the anomalies is 1981–2010. Correlations significant at the 90% level ($p < 0.1$) are circumscribed with a black line.

WR2 and WR5 both have weak correlations to SST_a in general, but show some very isolated locations where SST correlations are significant. The former regime is associated with positive z850 correlations (higher-than-normal geopotential height) over New Zealand and lower-than-normal pressure northeast of New Zealand in the subtropics close to the International Date Line (approximately where Fiji, Samoa, Niue, and Tonga are located). The latter regime, when increased in frequency, is associated with north central Tasman Sea low-pressure intensification (Figure 6) and cooler SST anomalies in the same area (Figure 5).

Correlations between WR monthly frequency anomalies and monthly SST anomalies at the Equator in the Pacific basin between 120°E and the South American coast (Figure 7; calculated using ERSSTv3c at 2° longitudinal increments) shows that WR6 has peak SST correlations at about 160°W and mostly strong correlations to the east of that location (a pattern corresponding to eastern Pacific types of El Niño). Both WR1 and WR3 have strong SST correlations for the central and western Pacific, but WR3 SST_a correlations are consistently stronger than WR1 eastwards from 170°E. Both WR2 and WR4 are poorly correlated to SSTs in the central Pacific. WR4 only has strong correlations to equatorial SST_a 20° either side of the International Date Line.

3.5. Relationships between WR and ENSO indices

Changes in WR probability for CEI phases (neutral phase is omitted for the sake of brevity: no significant modulations are found) along the seasonal cycle (Figure 8) show ocean-dominated ENSO events (Niño3.4 El Niño or Niño3.4 La Niña) are generally not associated with any significant WR frequency changes, bar a subtle increase in WR6 during austral summer–autumn. Conversely, both the atmosphere-dominated (SOI Niño/SOI Niña) and ocean–atmosphere aligned ENSO events (CEI Niño and CEI Niña) identified using the CEI indicate significant modulation of some WR frequencies. Overall, WR4 and WR5 do not appear to have appreciable correlations to the CEI, and only negative correlations for WR2 (i.e. a regime decrease) are only observed during SOI Niño events (Figure 8).

Prominent asymmetries for specific WR occurrences and for their preferred timing are highlighted for two main regime examples (WR3 and WR6; Section 3.4) that are suggested to have ENSO connections (Figure 8). WR3 is strongly decreased during CEI Niño (mainly during the austral spring, summer, and autumn period) but the same regime has weak increases during CEI Niña (for all times of the year except for DJF–FMA). Conversely, WR6 increases in association with CEI Niño and SOI Niño

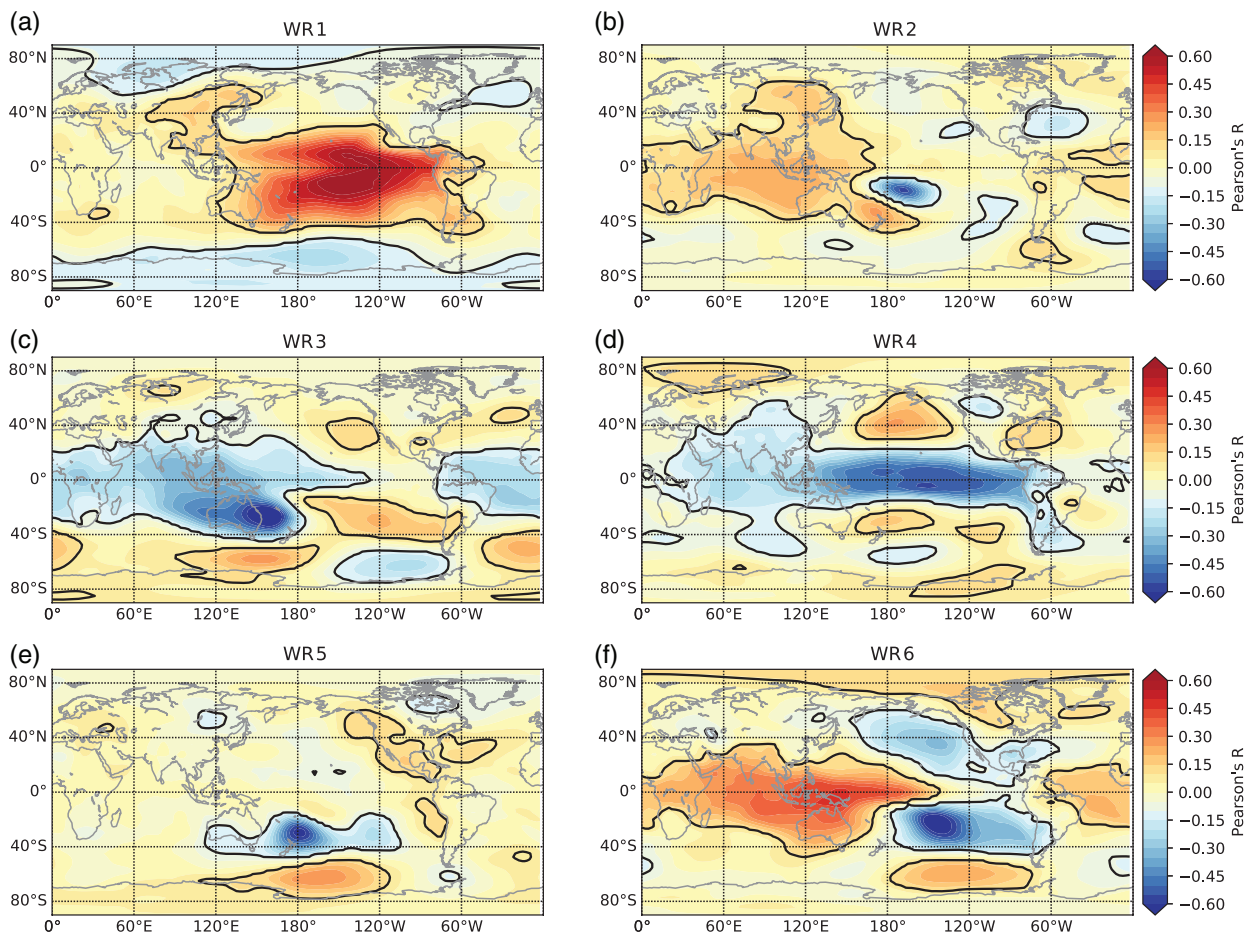


Figure 6. Correlation between SW Pacific atmospheric WR monthly frequency and the global monthly anomalies of Z850 (geopotential at 850 hPa). The climatological period for the calculation of the anomalies is 1981–2010. Correlations significant at the 90% level ($p < 0.1$) are circumscribed with a black line.

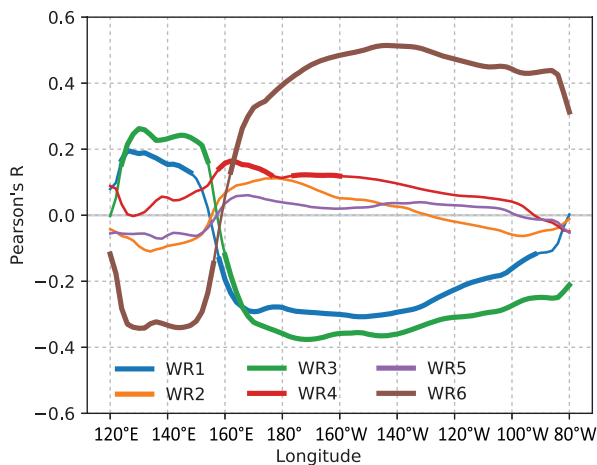


Figure 7. Correlation between SW Pacific atmospheric WRs and sea surface temperatures at the Equator (based on ERSSTv3c data) in 2° longitude increments.

phases, and it has a nearly opposite (symmetric) response (decrease in frequency) during CEI Niña and SOI Niña (Figure 8).

Interestingly, WR1 is also positively associated with SOI Niña and it has similar correlation patterns for SSTa as

what is observed for WR3 (Figure 5(c)). However, WR1 and WR3 have very different Pacific-wide geopotential patterns (Figures 6(a) and (c)). This shows that WRs with highly distinct atmospheric circulation patterns can be favoured during the same ENSO phase, and can also partly explain the variability of impacts between ENSO events of the same sign and similar magnitude as measured by only one index.

The changes in WR probability as a function of the EMI state ('neutral' category omitted because only weak and insignificant relationships were identified) and the phase of the seasonal cycle indicate the strongest and most significant frequency changes occur for WR1 (Figure 9). Increased occurrence of WR1, mostly during the SH late summer, autumn, winter, and early spring correspond to negative EMI phases (when SSTs in the central Pacific are anomalously cold). Conversely, during EMI positive phases, there is a much weaker change in the frequency of WR1 than what is observed during EMI negative conditions (Figure 9). WR3 has a robust positive frequency change when negative EMI conditions exist. It appears to strengthen during the time of the year (November–January and December–February) when no other observed strong relationships exist for the other WR. WR6 is also the only

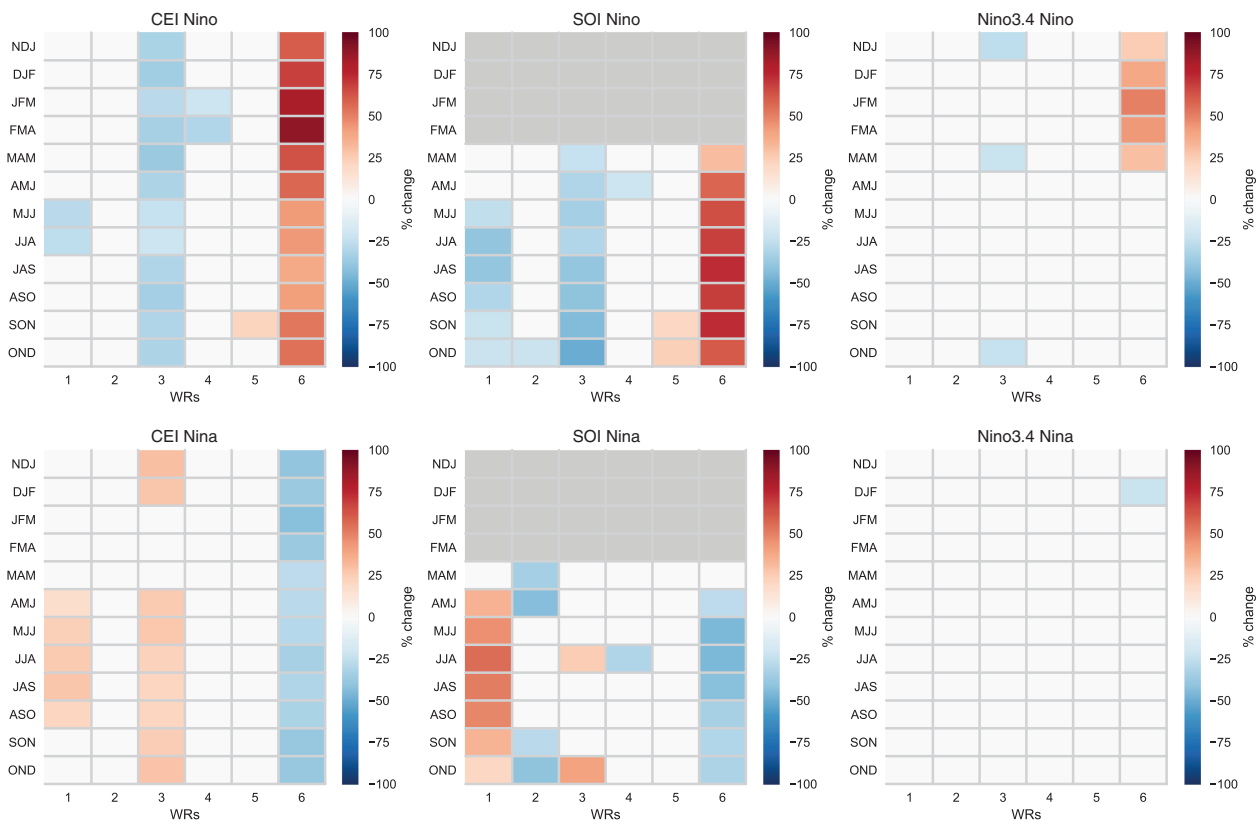


Figure 8. Seasonal changes for daily SW Pacific atmospheric WR frequency according to CEI phase. Two hundred percent indicates a doubling of the climatological frequency for each regime, 100% indicates no change, values below 100% indicate a decrease in the frequency compared to normal.

regime that appears to have a prominent association with positive EMI conditions.

WR4 and WR6 are reduced in frequency when negative EMI conditions exist during winter through early summer (Figure 9(a)). When positive EMI conditions occur, there appears to be no appreciable response from WR4, but as previously mentioned there is a response for WR6 during mid-winter through early summer and again for summer through early autumn (Figure 9(b)). WR2 is greatly reduced in frequency during mid-summer through mid-autumn when negative EMI conditions exist.

3.6. WR impacts on SP rainfall

The correlation between WR frequency and GPCP rainfall anomalies (1979–2014; all months combined) shows spatially distinct patterns across the SW Pacific region and outside the Pacific basin (Figures 10(a)–(f)). WR1 and WR3 (Figures 10(a) and (c), respectively) are previously ascribed as belonging to two distinct types of La Niña (Figures 5 and 8); yet again, these two regimes exhibit subtly different tropical and extra-tropical correlation patterns. For WR3 the SPCZ is inferred to move south and west of normal based on negative correlations (drying) in a diagonally orientated zone aligned to the location where the SPCZ normally sits, coupled with positive correlations (relative wetting) near the Maritime Continent, the Coral Sea, and over New Caledonia. Conversely, the GPCP correlation maps (Figure 10(f)) indicate WR6

(shown as the opposite of WR3, Figures 5 and 6) has the most prominent, large-scale positive rainfall anomalies spread across the SW Pacific tropics, but also suggests distinct dry anomalies occur in the area around the Coral Sea, New Caledonia and in the subtropical zone around the International Date Line (encompassing Fiji, Tonga, and Niue). Positive rainfall correlations associated with WR6 indicate enhanced precipitation along the Equator around and east of the IDL and decreased rainfall over the Maritime Continent and in the southwest Pacific (from Papua New Guinea southeast to east of Fiji). The correlation field for WR6 suggests the SPCZ shifts north and east of normal. WR1 indicates relative drying occurs within regions usually occupied by both the ITCZ and SPCZ (Figure 10(a)). WR4 strongest correlations suggest it is associated with an enhanced ITCZ (Figure 10(d)), which is not surprising given the associated geopotential height anomalies that comprise this regime (Figure 6). WR4 frequency increases are associated with increased rainfall parallel to the northern side of the Equator from the Maritime Continent to about 110°W and decreased precipitation south of the Equator from about the International Date Line east to South America (Figure 10(d)). WR2 has a strong positive and negative precipitation ‘dipole’ correlation signature that is localized between the Coral Sea and French Polynesia (Figure 10(b)). WR2 is also associated with the strongest rainfall anomalies along the Equator for areas east of the International Date

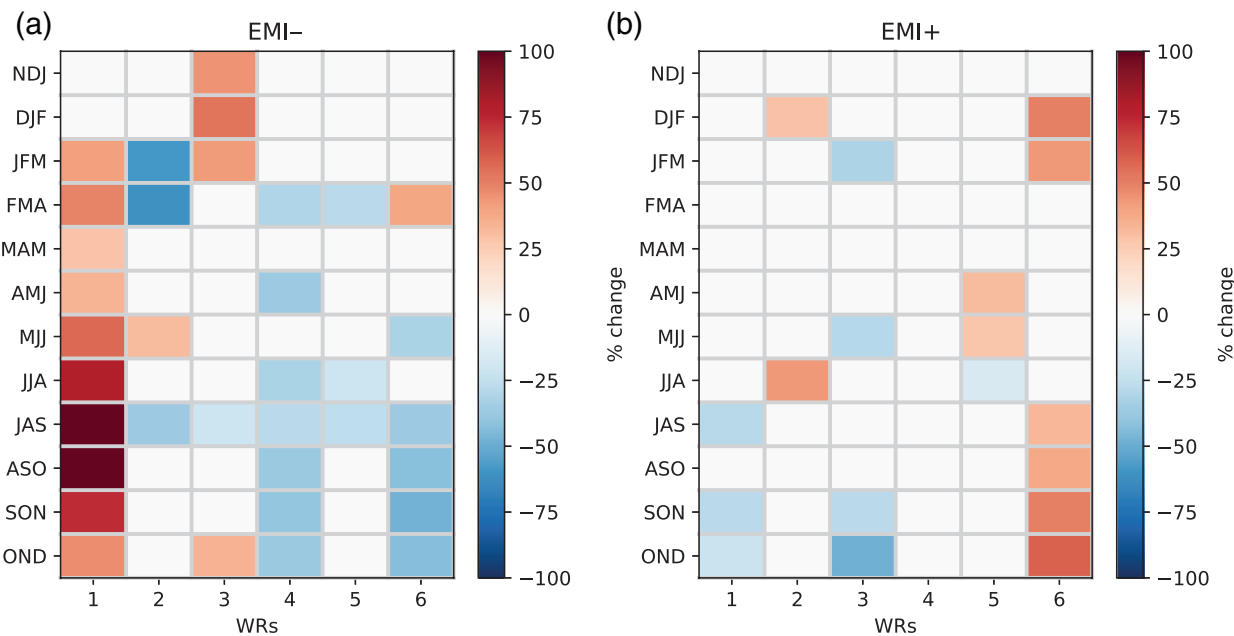


Figure 9. Rolling 3-month EMI negative and positive associations of southwest Pacific atmospheric WR frequency changes.

Line, along with WR6. The correlations for GPCP rainfall anomalies associated with WR5 are mostly near-normal over most of the SW Pacific tropics, and any appreciable correlation anomalies are confined to the subtropical and mid-latitudes of the SP basin (Figure 10(e)).

Local *in situ* rainfall variability at a seasonal level can be connected to WR frequency changes (Figure 11). Using a network of stations with high-quality rain data for austral summer (December, January, February) spanning the SW Pacific domain (and some sites just outside of it; Cairns, Townsville, Sydney, and Kaitaia), distinct spatial patterns are observed for seasonal rainfall correlations to each regime (Figure 11). The strongest correlation of rainfall at any one site to a regime was observed for Hiva‘Oa in the Marquesas and WR6 (Figure 11(f)), closely followed by Salote (Tonga) and WR3 (Figure 11(c)). Of the selected island rainfall analysed in this study, Takaroa (in the Tuamotu Archipelago) shows a significant correlation to four WRs during summer, and most other island rainfall–WR correlations are significant for one to three WRs (with the surprising exception of Tahiti). Based on the number of sites that had significant correlations between WR occurrence and *in situ* rainfall totals, WR3 and WR6 appear to be the most important across the region, followed by WR2 and WR1. WR5 only appears to have an important effect during summer on Apia rainfall, and WR4 has no significant correlation to any of the stations assessed in this study. The poorest correlations between *in situ* rainfall totals and WR frequency for the analysed sites were observed for Cairns, Townsville, Sydney, and Kaitaia. Overall, the variable strength of these correlations indicate that any one regime may or may not play a strong role in the overall variability of summer season rainfall at any given site we analysed (in some cases, it is strong, while others it is weak).

However, when *in situ* island rainfall anomalies were aggregated by decile of WR occurrence (D1 indicates the lowest regime frequency and vice versa for D10), the average percent of normal seasonal rainfall illustrates stark outcomes for dryness and wetness in response to WR changes (Figure 11). We do not isolate the impact of any one WR on the rainfall anomalies here and recognize that they co-occur to bring about seasonal climate conditions. However, what emerges from this analysis is that WR occurrence plays a strong role in dictating extreme seasonal rainfall for some SW Pacific locations. The greatest differences between average summer rainfall anomalies associated for D1 and D10 WR occurrence is observed for Hiva‘Oa (Marquesas) in response to changes in WR1, WR4, WR5, and WR6, for Noumea (New Caledonia) in response to WR3, and for Tarawa (Kiribati) in response to WR2 changes. The strongest negative rainfall anomalies in response to an overall regime increase occurs for Tarawa (with an average of 25% normal DJF rainfall) when WR3 is greatly increased, while the strongest positive rainfall anomalies are observed for Hiva‘Oa (with an average of 228% normal DJF rainfall) in association with increased occurrence of WR6.

4. Discussion

4.1. Association of WRs with ENSO

The repeated AP exercise has reduced daily weather in the SW Pacific domain to six recurrent WRs (Figure 1) that have been analysed in this study. We demonstrate that some of the regimes (Figure 2), but not all, appear sensitive to oceanic and atmospheric components of ENSO activity. We also observe that there is a phase-locking of some WR to the annual cycle (Figure 3). However, some of the characteristic traits seen in climate field correlations

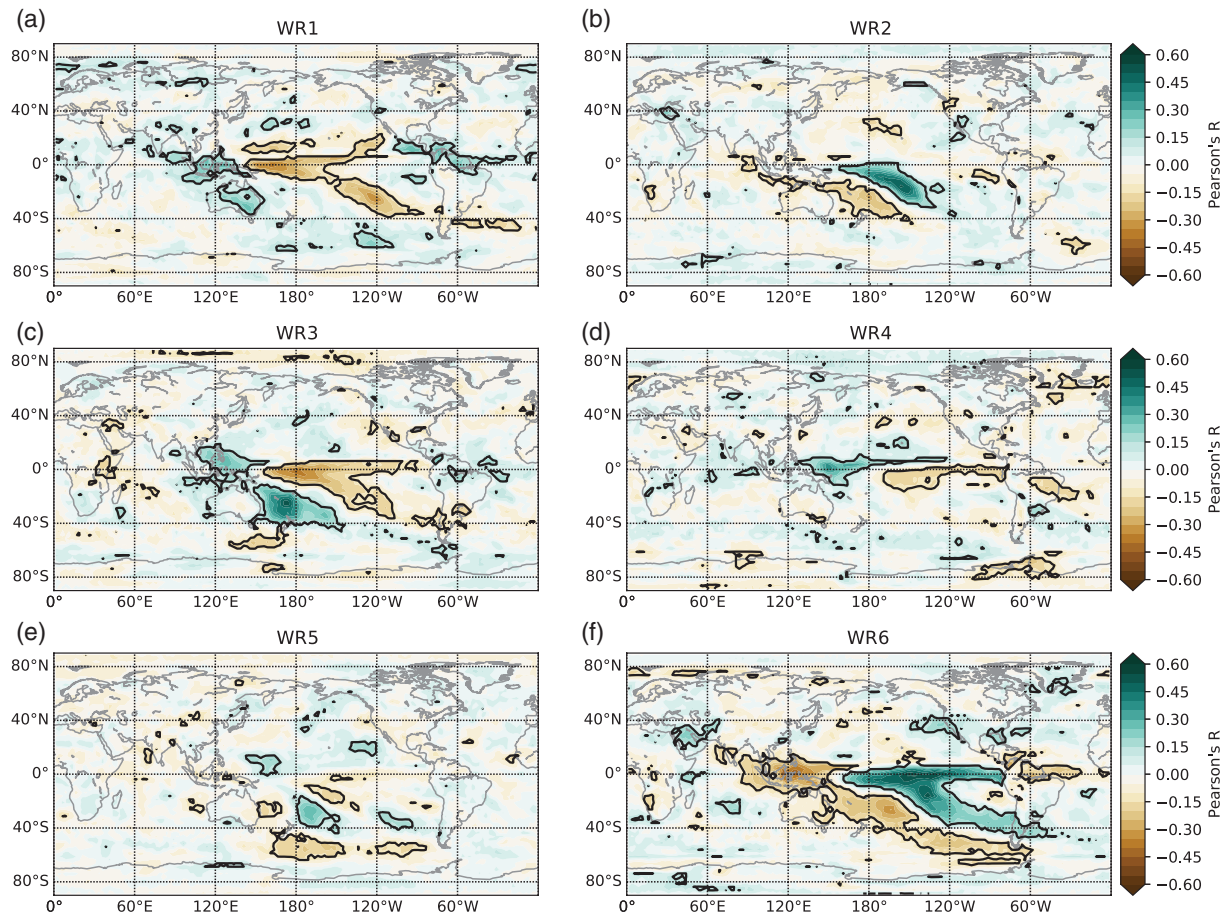


Figure 10. Correlation between daily southwest Pacific atmospheric WR frequency changes and precipitation anomalies from the GPCP. The climatological period for the calculation of the anomalies is 1981–2010. Correlations significant at the 90% level ($p < 0.1$) are contoured. Positive (negative) rainfall anomalies are associated with a regime increase (decrease).

that are related to each of the regimes (Figures 5 and 6) appear unrelated to ENSO, and may therefore suggest that they arise from other climate modes (following section) or internal atmospheric variability.

The spatial expression for WR1, WR3, and WR6 to SST in patterns that are akin to those seen for ENSO (e.g. Allan *et al.*, 1996) strongly suggests that (unsurprisingly) ENSO is a major contributor to WR variability in the SW Pacific. The connection of some WRs to ENSO reflects the SW Pacific geographic domain choice that was made in this study (Appendix S1), and the overlap of the domain with core regions of ENSO operation – namely the Niño3.4 zone, the eastern edge of the Indo-Pacific warm pool and one of the atmospheric poles of the Southern Oscillation. Our reasoning for this domain choice was to locate the SPCZ in the middle of the field of analysis because of its relevance to small Pacific Islands. It is also evident that some WR occurrences and their climatological characteristics (Figure 3) are related to the growth and decay of ENSO events (McPhaden *et al.*, 2006). For instance, the regimes that are associated with CEI ENSO (WR3, WR6, and to a lesser extent WR1; Figure 8) exhibit a rise and fall of frequency as well as self-persistence (Figure 4(c)) that are locked to the annual cycle, which is also known to modulate the strength of ENSO with a similar timing.

Two ‘opposite’ WRs appear closely linked to CEI ENSO (WR3; ‘TNT’ and WR6; ‘TFP’; Figure 2). They show highly, but not exactly, contrasting spatial correlation patterns (Figures 5, 6, and 10). The contrasts between the CEI-based and EMI-based analyses (Figures 8 and 9) also suggest ENSO forcing of WR frequency changes are probably more prevalent when linked ocean–atmosphere situations are strongest during spring through autumn (i.e. when both atmospheric and oceanic anomalies related to ENSO are prevalent). For Equatorial Pacific ocean-dominated ENSO events (as with La Niña Modoki), autumn through early summer WR changes may be more common (Figure 8). In the latter situation, however, we note that there is not an ‘opposite’ regime that has been identified as a counterpart to what associates with La Niña Modoki (WR1; ‘HSP’); however, this could be due to the choice of restricting our analysis domain to the central western Pacific (i.e. if the far eastern Pacific had been included better encompassing a main activity region of eastern Pacific El Niño, then perhaps a distinct regime linked to El Niño Modoki may have been identified).

There is a discernable ENSO connection for WR1 during austral winter when SOI Niño and SOI Niña conditions exist. Despite WR1 also having strong SST correlations nearly equivalent to WR3 across the

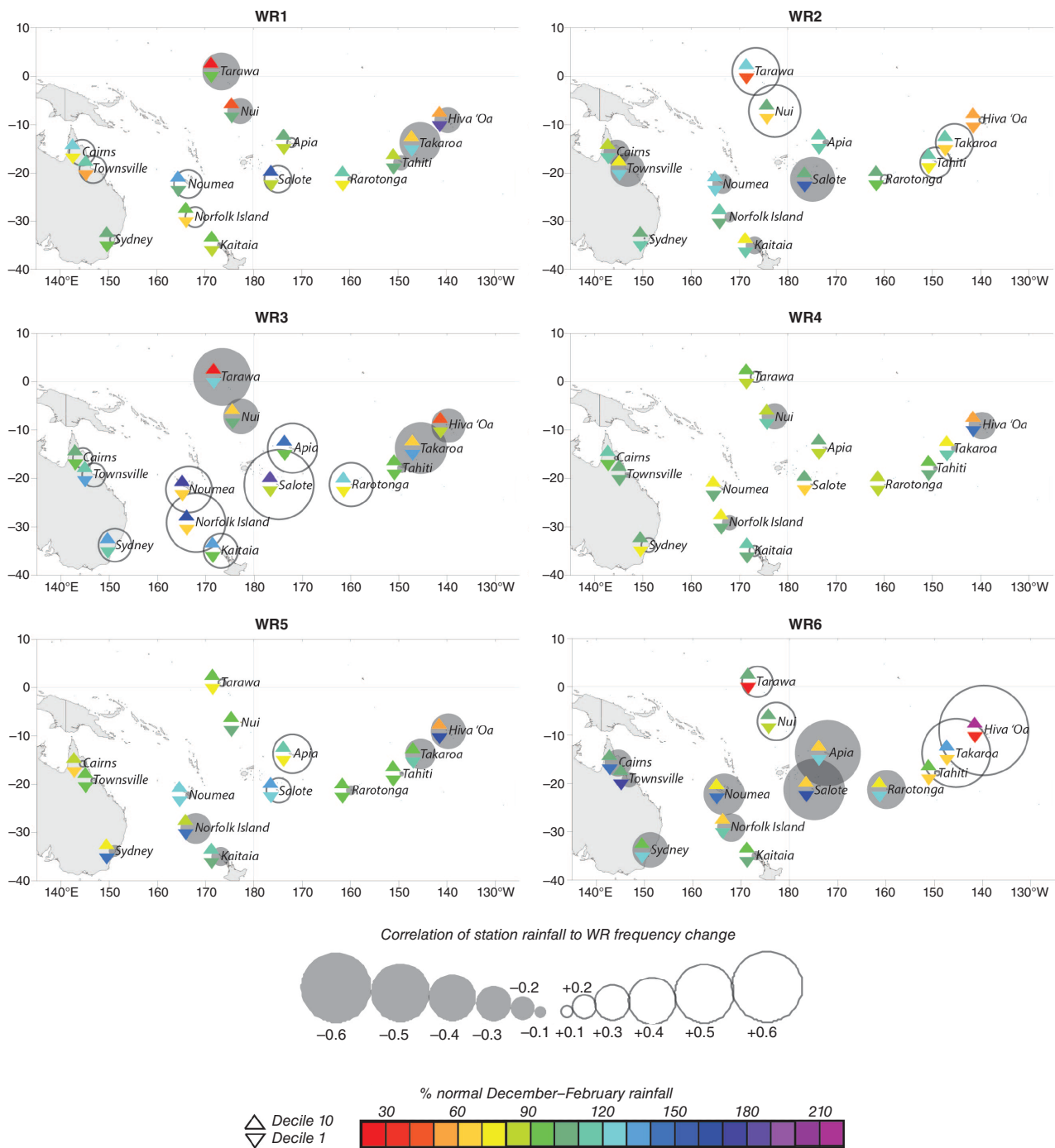


Figure 11. Correlation between southwest Pacific atmospheric WR frequency and *in situ* rainfall anomalies for December–February at selected Pacific Island stations for 1950–1951 to 2013–2014. The period for calculating the seasonal climatology values is 1981–2010. Correlations significant at the 99% level ($p < 0.01$) exceeded $r = \pm 0.32$.

Equatorial Pacific (Figure 7), the main differentiation between those two regimes relates to regional atmospheric features (Figure 2), which is also reflected in wider geopotential height correlation patterns (Figure 6). The differences between the spatial correlation fields for these two WRs are strikingly similar (and correspond to other metrics) ascribed recently by Song *et al.* (2016) for two types of La Niña; and as such we relate WR1 as arising more frequently during central Pacific La Niña and WR3 increases as related to eastern Pacific La Niña events.

Distinct spatial differences for the WR impacts on *in situ* rainfall (Figure 11) are likely connected to associated movements of the ITCZ and SPCZ, which are respond to the SW Pacific atmospheric circulation (Lorrey *et al.*, 2012a for summer rainfall patterns linked to CEI phases). In addition, subtle differences between ENSO flavours are known to modulate region-wide tropical cyclone characteristics (Diamond *et al.*, 2013). Therefore, ENSO should realistically play a significant role in the wider spatial patterns that are associated with the WRs, while also

helping to dictate the specific rainfall anomalies for different small island nations in the SW Pacific region (Figure 10). Further work to examine inter-annual variability on the WR impacts and specific orographic signatures is also warranted.

4.2. Extra-basin and extra-tropical influences on SW Pacific atmospheric WRs

In some cases, the correlation maps for z850 and SSTa show subtle spatial pattern characteristics that appear similar to the signatures of known climate phenomena, with strong anomalies outside of the tropical Pacific region. This indicates that climate driver influences from outside the Pacific basin may contribute to SW Pacific WR formation, and these drivers may result in influences on regional weather via teleconnections (Liu and Alexander, 2007). However, further work would be required to establish the physical mechanisms that potentially support these teleconnections. A brief elaboration based on the observed spatial fields (Figures 5 and 6) for WR2 and WR5 is provided in this discussion in light of prior work that demonstrates multiple climate driver teleconnections from distal sources can affect some Pacific weather types (Jiang *et al.*, 2013).

In the z850 correlation field that is associated with WR2 (Figure 6(b)), an increase in regime frequency is concurrent with higher-than-normal geopotential heights over the entire Indian Ocean basin, the Maritime Continent, and the Indo-Pacific warm pool (as well as New Zealand) with strong low pressure northeast of New Zealand. This geopotential height pattern appears similar to what develops at the tail end of the MJO, so we examined WR2 frequency changes and the MJO index. WR2 is significantly increased (frequency nearly doubled) during MJO phase 7 (Figure 12), suggesting it is triggered as MJO convective pulses enter the Pacific basin. The correspondence of the geopotential height signatures for WR2 (Figures 2 and 6) and increases in associated rainfall in the Tropics and subtropics (where outgoing long-wave radiation signatures are negative for MJO phase 7; Figure 12) lends to the assertion that WR2 arises largely from the end of discrete MJO cycles as they draw to a close in the SW Pacific (Wheeler and Hendon, 2004).

WR5 also has a strong ‘high’ centred in the Ross Sea sector, and climatologically this regime occurs with greater frequency during late austral autumn (May) through mid austral spring (October). The mid-to-high-latitude expression of the z850 correlation field for the New Zealand and Ross sea sector of the Southern Ocean (Figure 6(e)) suggests this may represent a Southern Annular Mode (SAM) influence on WR5 (Fogt and Bromwich, 2006; Fogt *et al.*, 2011, 2012). Correlations for SST appear weak outside of the Pacific basin, but those signatures that are strong suggest in-flow of warmer SST into the north Tasman Sea via the East Australian Current would be inhibited, promoting cooler waters when WR5 occurs because of the southerly wind stress across the Tasman Sea sector. There are also aspects of the WR1 spatial

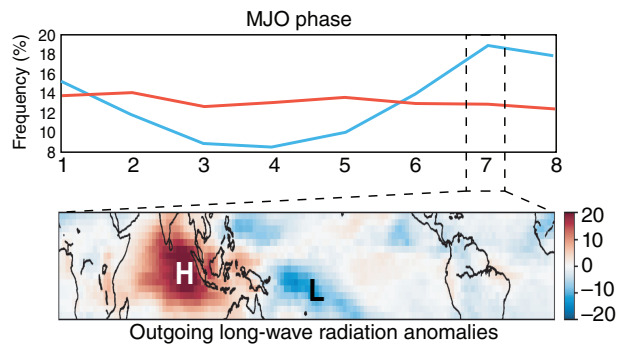


Figure 12. (top) Percent frequency change of MJO phases (blue line) with respect to WR2 ('STL' type) compared to MJO phase climatological frequency (red line) and (bottom) MJO phase 7 outgoing long-wave radiation spatial anomalies (w m^{-2}). ‘H’ and ‘L’ indicate locations of high and low anomalous geopotential height seen in z850 (Figure 6), respectively. Blue shades are where more cloud cover would be located.

correlations that are reminiscent of SAM (with regard to a broadly annular pattern circumscribing Antarctica) that are reminiscent of what can occur in concert with La Niña.

WR3 and WR6 (connected to ENSO; see previous section) also both exhibit an significant Antarctic dipole z850 correlation pattern that is positioned in a configuration reminiscent of the PSA (Mo and Paegle, 2001). The PSA typically exhibits a see-saw in atmospheric mass between the Amundsen–Bellinghausen sector west of the Drake Passage and the South Indian Ocean–western Ross Sea sector of the Southern Ocean along the Antarctic continent margin. This association is not surprising, but future work that focuses on the relationships between SW Pacific WRs and climate drivers external to the Pacific basin would help shed more light on these possible linkages. In addition, further analysis of how low-, mid-, and high-latitude synoptic types transition between one another, and their lead and lag relationships may help better understand potential atmospheric teleconnections and predictability on sub-seasonal time scales.

5. Conclusions

The *k*-means clustering analysis applied to daily near-surface geopotential fields has allowed a basic categorization and characterization of SW Pacific atmospheric WRs (Figure 2). The WR are important as they are ‘attractors’ for discrete types of weather (dry, wet, warm, cool, etc.). When aggregated over monthly and longer time scales (Ghil and Robertson, 2002), WRs appear capable of producing significant seasonal climate impacts for small Pacific islands (droughts, pluvials, etc.). We have illustrated that a significant proportion of the WRs are related to ENSO, to fundamental global atmospheric circulation properties (Hadley–Ferrell circulation), and to climate modes that have core elements outside the SW Pacific region (MJO, PSA, SAM). There are not always diametrically opposite occurrences of WR changes for different flavours of ENSO, and there is not always a single climate phenomenon that is responsible for a WR

waxing and waning in importance over the course of the annual cycle. Complex interplays of several climate teleconnections clearly help to exert important influences on SW Pacific weather types. Nevertheless, the classification that has been established in this study will allow a link between these regimes and distinct rainfall outcomes for Pacific Islands in future studies, which is expected to assist weather and seasonal climate forecasting of extreme precipitation (Kruk *et al.*, 2015), temperatures for sea surface and land, as well as wind flow patterns.

An additional application of this study is towards regional palaeoclimate reconstruction efforts that employ atmospheric circulation regimes for integrating disparate climate archive signals (Lorre *et al.*, 2007, 2008, 2012b; Goodwin *et al.*, 2014a; Lorrey *et al.*, 2014a; Browning and Goodwin, 2015). As such, the WR classification produced here is expected to assist Hemisphere-wide palaeodata interpretation where large data sets are employed (see Past Global Changes (PAGES) 2k Consortium (2013) for a recent example as well as the International Quaternary Union (INQUA) supported Southern Hemisphere Assessment of PalaeoEnvironments (SHAPE) international focus group). Moreover, extensive evidence demonstrates significant terrestrial, marine, and human changes occurred across the Pacific region during the last millennium that may be due to weather and climate variability (Goodwin *et al.*, 2014b); however, connections of past changes in weather to climate processes have been underdeveloped. The continued effort to link archaeological records to local climate reconstructions that can provide meaningful insight about knock-on impacts to subsistence economies has previously proved difficult as well, in part, because Pacific data are widely spaced and are relatively limited across Oceania. The advances made from this work, when applied to emerging regional palaeoclimatology proxy data and archaeology data networks, may also help to highlight the changeable influences of ENSO, extra-tropical and extra-Pacific basin climate processes and dynamics on Pacific Islands. Given the significant rainfall anomalies observed for the Marquesas, Samoa, Tonga, and Tahiti station data used in this study, which all come from islands with rich records of pre-historic occupation and change (Allen, 2006), we would suggest future palaeoclimatology–archaeology linkages could be enhanced using a SW Pacific atmospheric WR context.

The outlook for ENSO activity under warming global conditions and the fate of the Pacific Islands from future ENSO impacts is not totally certain (Wang and Cai, 2013; Cai *et al.*, 2015). However, some leading hypotheses indicate the surface and atmospheric variability associated with ENSO will increase (Cai *et al.*, 2012; Fowler *et al.*, 2012). As such, an interrogation of climate model simulation data that examines how WRs shift under different greenhouse gas representative concentration pathways (Collins *et al.*, 2013) could provide a new perspective of what the future may hold for the SW Pacific. A WR interrogation of climate model simulations might also offer an additional perspective to assist in making large-scale atmospheric circulation patterns more compatible with

small-island-scale climate responses, especially where orographic influences are strong. In addition, SPCZ movements under future scenarios are notoriously variable in future simulations (Brown *et al.*, 2012). Therefore, our suggestion to analyse WRs in climate model simulations may also assist in improving climate model selection or help to improve weighting for ensemble-based projections of future effective precipitation changes.

Acknowledgements

This work is a contribution to the Royal Society of New Zealand Marsden Fund project ‘Detecting prehistoric human–climate dynamics in central Polynesia using high-precision marine archives’. Co-funding for AML and NCF time for analysis also came from the NIWA core-funded project ‘Climate Present and Past’ project CAOA1701 and NOAA support for ‘The South Pacific Rainfall Atlas (SPRAT)’. John-Mark Woolley is thanked for processing rainfall data.

Supporting information

The following supporting information is available as part of the online article:

Appendix S1. Choice of the domain and the variable, and sensitivity to the domain choice.

References

- Ackerley D, Lorrey A, Renwick JA, Phipps SJ, Wagner S, Dean S, Singarayer J, Valdes P, Abe-Ouchi A, Ohgaito R, Jones JM. 2011. Using synoptic type analysis to understand New Zealand climate during the mid-Holocene. *Clim. Past* **7**(4): 1189–1207.
- Adler RF, Huffman GJ, Chang A, Ferraro R, Xie PP, Janowiak J, Rudolf B, Schneider U, Curtis S, Bolvin D, Gruber A. 2003. The version-2 global precipitation climatology project (GPCP) monthly precipitation analysis (1979–present). *J. Hydrometeorol.* **4**(6): 1147–1167.
- Allan R, Lindesay J, Parker D. 1996. *El Niño Southern Oscillation and Climatic Variability*. CSIRO Publishing: Melbourne.
- Allen MS. 2006. New ideas about late Holocene climate variability in the central Pacific. *Curr. Anthropol.* **47**(3): 521–535.
- Ashok K, Behera SK, Rao SA, Weng H, Yamagata T. 2007. El Niño Modoki and its possible teleconnection. *J. Geophys. Res. Oceans* **112**: C11007. <https://doi.org/10.1029/2006JC003798>.
- Baldwin MP, Dunkerton TJ. 2001. Stratospheric harbingers of anomalous weather regimes. *Science* **294**(5542): 581–584.
- Brown JR, Moise AF, Delange FP. 2012. Changes in the South Pacific convergence zone in IPCC AR4 future climate projections. *Clim. Dyn.* **39**: 1–19.
- Browning SA, Goodwin ID. 2015. The paleoclimate reanalysis project. *Clim. Past Discuss.* **11**: 4159–4204.
- Cai W, Lengaigne M, Borlace S, Collins M, Cowan T, McPhaden MJ, Timmermann A, Power S, Brown J, Menkes C, Ngari A. 2012. More extreme swings of the South Pacific convergence zone due to greenhouse warming. *Nature* **488**(7411): 365–369.
- Cai W, Santoso A, Wang G, Yeh SW, An SI, Cobb KM, Collins M, Guilyardi E, Jin FF, Kug JS, Lengaigne M. 2015. ENSO and greenhouse warming. *Nat. Clim. Change* **5**: 849–859. <https://doi.org/10.1038/nclimate2743>.
- Capotondi A, Wittenberg AT, Newman M, Di Lorenzo E, Yu JY, Braconnot P, Cole J, Dewitte B, Giese B, Guilyardi E, Jin FF. 2015. Understanding ENSO diversity. *Bull. Am. Meteorol. Soc.* **96**(6): 921–938.
- Cassou C. 2008. Intraseasonal interaction between the Madden–Julian oscillation and the North Atlantic oscillation. *Nature* **455**(7212): 523–527.

- Collins M, Knutti R, Arblaster J, Dufresne J-L, Fichefet T, Friedlingstein P, Gao X, Gutowski WJ, Johns T, Krinner G, Shongwe M, Tebaldi C, Weaver AJ, Wehner M. 2013. Long-term climate change: projections, commitments and irreversibility. In *Climate Change 2013: The Physical Science Basis. Contribution of Working Group I to the Fifth Assessment Report of the Intergovernmental Panel on Climate Change*, Stocker TF, Qin D, Plattner G-K, Tignor M, Allen SK, Boschung J, Nauels A, Xia Y, Bex V, Midgley PM (eds). Cambridge University Press: Cambridge, UK and New York, NY.
- Diamond HJ, Lorrey AM, Renwick JA. 2013. A southwest Pacific tropical cyclone climatology and linkages to the El Niño–Southern Oscillation. *J. Clim.* **26**(1): 3–25.
- Fauchereau N, Pohl B, Lorrey A. 2016. Extratropical impacts of the Madden–Julian oscillation over New Zealand from a weather regime perspective. *J. Clim.* **29**(6): 2161–2175.
- Fog RL, Bromwich DH. 2006. Decadal variability of the ENSO teleconnection to the high-latitude South Pacific governed by coupling with the southern annular mode. *J. Clim.* **19**(6): 979–997.
- Fog RL, Bromwich DH, Hines KM. 2011. Understanding the SAM influence on the South Pacific ENSO teleconnection. *Clim. Dyn.* **36**(7–8): 1555–1576.
- Fog RL, Jones JM, Renwick J. 2012. Seasonal zonal asymmetries in the southern annular mode and their impact on regional temperature anomalies. *J. Clim.* **25**: 6253–6270. <https://doi.org/10.1175/JCLI-D-11-00474.1>.
- Fowler AM, Boswijk G, Lorrey AM, Gergis J, Pyrie M, McCloskey SPJ, Palmer JG, Wunder J. 2012. Significant ENSO changes in a warmer world suggested by New Zealand forest giants. *Nat. Clim. Change* **2**: 172–176.
- Frey BJ, Dueck D. 2007. Clustering by passing messages between data points. *Science* **315**(5814): 972–976.
- Gergis JL, Fowler AM. 2005. Classification of synchronous oceanic and atmospheric El Niño–Southern Oscillation (ENSO) events for palaeoclimate reconstruction. *Int. J. Climatol.* **25**(12): 1541–1565.
- Ghil M, Robertson AW. 2002. “Waves” vs. “particles” in the atmosphere’s phase space: a pathway to long-range forecasting? *Proc. Natl. Acad. Sci. U.S.A.* **99**: 2493–2500. <https://doi.org/10.1073/pnas.012580899>.
- Goodwin ID, Browning S, Lorrey AM, Mayewski PA, Phipps SJ, Bertler NA, Edwards RP, Cohen TJ, van Ommen T, Curran M, Barr C. 2014a. A reconstruction of extratropical Indo-Pacific sea-level pressure patterns during the Medieval climate anomaly. *Clim. Dyn.* **43**(5–6): 1197–1219.
- Goodwin ID, Browning SA, Anderson AJ. 2014b. Climate windows for Polynesian voyaging to New Zealand and Easter Island. *Proc. Natl. Acad. Sci. U.S.A.* **111**(41): 14716–14721. <https://doi.org/10.1073/pnas.1408918111>.
- Hartigan JA. 1975. *Clustering Algorithms*. Wiley: New York, NY.
- Jiang N, Griffiths G, Lorrey A. 2013. Influence of large-scale climate modes on daily synoptic weather types over New Zealand. *Int. J. Climatol.* **33**(2): 499–519.
- Johnson NC. 2013. How many ENSO flavors can we distinguish? *J. Clim.* **26**(13): 4816–4827.
- Kalnay E, Kanamitsu M, Kistler R, Collins W, Deaven D, Gandin L, Iredell M, Saha S, White G, Woollen J, Zhu Y. 1996. The NCEP/NCAR 40-year reanalysis project. *Bull. Am. Meteorol. Soc.* **77**(3): 437–471.
- Kaufman L, Rousseeuw PJ. 1990. *Finding Groups in Data: an introduction to cluster analysis*. John Wiley and Sons: Hoboken, NJ.
- Kidson JW. 2000. An analysis of New Zealand synoptic types and their use in defining weather regimes. *Int. J. Climatol.* **20**(3): 299–316.
- Kimoto M. 1989. *Multiple Flow Regimes in the Northern Hemisphere Winter*. PhD thesis, University of California, Los Angeles, CA, 210 pp.
- Kruk MC, Lorrey AM, Griffiths GM, Lander M, Gibney EJ, Diamond HJ, Marra JJ. 2015. On the state of the knowledge of rainfall extremes in the western and northern Pacific basin. *Int. J. Climatol.* **35**(3): 321–336.
- Kug JS, Jin FF, An SI. 2009. Two types of El Niño events: cold tongue El Niño and warm pool El Niño. *J. Clim.* **22**(6): 1499–1515.
- Larkin NK, Harrison DE. 2005. Global seasonal temperature and precipitation anomalies during El Niño autumn and winter. *Geophys. Res. Lett.* **32**: L16705. <https://doi.org/10.1029/2005GL022860>.
- Lefèvre J, Marchesiello P, Jourdain NC, Menkes C, Leroy A. 2010. Weather regimes and orographic circulation around New Caledonia. *Mar. Pollut. Bull.* **61**(7): 413–431.
- Liu Z, Alexander M. 2007. Atmospheric bridge, oceanic tunnel, and global climatic teleconnections. *Rev. Geophys.* **45**: RG2005. <https://doi.org/10.1029/2005RG000172>.
- Lorrey A, Renwick J. 2011. Assessment of the 2010–11 southwest Pacific drought. NIWA Client Report AKL2011-036, New Zealand Ministry of Foreign Affairs and Trade, 20 pp.
- Lorrey A, Fowler AM, Salinger J. 2007. Regional climate regime classification as a qualitative tool for interpreting multi-proxy palaeoclimate data spatial patterns: a New Zealand case study. *Palaeogeogr. Palaeoclimatol. Palaeoecol.* **253**(3): 407–433.
- Lorrey A, Williams P, Salinger J, Martin T, Palmer J, Fowler A, Zhao JX, Neil H. 2008. Speleothem stable isotope records interpreted within a multi-proxy framework and implications for New Zealand palaeoclimate reconstruction. *Quat. Int.* **187**(1): 52–75.
- Lorrey AM, Vandergoes M, Almond P, Renwick J, Stephens T, Bostock H, Mackintosh A, Newnham R, Williams PW, Ackerley D, Neil H. 2012a. Palaeocirculation across New Zealand during the last glacial maximum at ~21 ka. *Quat. Sci. Rev.* **36**: 189–213.
- Lorrey A, Dalu G, Renwick J, Diamond H, Gaetani M. 2012b. Reconstructing the South Pacific convergence zone position during the presatellite era: a La Niña case study. *Mon. Weather Rev.* **140**(11): 3653–3668.
- Lorrey A, Fauchereau N, Stanton C, Chappell P, Phipps S, Mackintosh A, Renwick J, Goodwin I, Fowler A. 2014a. The Little Ice Age climate of New Zealand reconstructed from southern Alps cirque glaciers: a synoptic type approach. *Clim. Dyn.* **42**(11–12): 3039–3060.
- Lorrey AM, Griffiths G, Fauchereau N, Diamond HJ, Chappell PR, Renwick J. 2014b. An ex-tropical cyclone climatology for Auckland, New Zealand. *Int. J. Climatol.* **34**: 1157–1168.
- Matthews AJ. 2012. A multiscale framework for the origin and variability of the South Pacific convergence zone. *Q. J. R. Meteorol. Soc.* **138**(666): 1165–1178.
- McPhaden MJ, Zebiak SE, Glantz MH. 2006. ENSO as an integrating concept in earth science. *Science* **314**(5806): 1740–1745.
- Michelangeli PA, Vautard R, Legras B. 1995. Weather regimes: recurrence and quasi stationarity. *J. Atmos. Sci.* **52**(8): 1237–1256.
- Mo K, Ghil M. 1988. Cluster analysis of multiple planetary flow regimes. *J. Geophys. Res.* **93**(9): 10927–10952.
- Mo KC, Paegle JN. 2001. The Pacific–South American modes and their downstream effects. *Int. J. Climatol.* **21**(10): 1211–1229.
- Moron V, Plaut G. 2003. The impact of El Niño–Southern Oscillation upon weather regimes over Europe and the North Atlantic during boreal winter. *Int. J. Climatol.* **23**(4): 363–379.
- Moron V, Gouirand I, Taylor M. 2016. Weather types across the Caribbean basin and their relationship with rainfall and sea surface temperature. *Clim. Dyn.* **47**(1–2): 601–621. <https://doi.org/10.1007/s00382-015-2858-9>.
- Park HS, Jun CH. 2009. A simple and fast algorithm for K-medoids clustering. *Expert Syst. Appl.* **36**(2): 3336–3341.
- Past Global Changes (PAGES) 2k Consortium. 2013. Continental-scale temperature variability during the past two millennia. *Nat. Geosci.* **6**: 339–346. <https://doi.org/10.1038/ngeo1797>.
- Qian W, Shan X, Chen D, Zhu C, Zhu Y. 2012. Droughts near the northern fringe of the East Asian summer monsoon in China during 1470–2003. *Clim. Change* **110**(1–2): 373–383.
- Renwick JA. 2011. Kidson’s synoptic weather types and surface climate variability over New Zealand. *Weather Clim.* **31**: 3–23.
- Riddle EE, Stoner MB, Johnson NC, L’Heureux ML, Collins DC, Feldstein SB. 2013. The impact of the MJO on clusters of wintertime circulation anomalies over the North American region. *Clim. Dyn.* **40**(7–8): 1749–1766.
- Song L, Chen S, Chen W, Chen X. 2016. Distinct impacts of two types of La Niña events on Australian summer rainfall. *Int. J. Climatol.* **37**: 2532–2544. <https://doi.org/10.1002/joc.4863>.
- Troup AJ. 1965. The “southern oscillation.” *Q. J. R. Meteorol. Soc.* **102**: 490–506.
- Tziperman E, Stone L, Cane MA, Jarosh H. 1994. El Niño chaos: overlapping of resonances between the seasonal cycle and the Pacific ocean-atmosphere oscillator. *Science* **264**(5155): 72–74.
- Vautard R. 1990. Multiple weather regimes over the North Atlantic: analysis of precursors and successors. *Mon. Weather Rev.* **118**(10): 2056–2081.
- Vautard R, Legras B. 1988. On the source of midlatitude low-frequency variability. Part II: nonlinear equilibration of weather regimes. *J. Atmos. Sci.* **45**(20): 2845–2867.

- Vincent EM, Lengaigne M, Menkes CE, Jourdain NC, Marchesiello P, Madec G. 2011. Interannual variability of the South Pacific convergence zone and implications for tropical cyclone genesis. *Clim. Dyn.* **36**: 1881–1896.
- Wang G, Cai W. 2013. Climate-change impact on the 20th-century relationship between the southern annular mode and global mean temperature. *Sci. Rep.* **3**: 2039. <https://doi.org/10.1038/srep02039>.
- Wheeler M, Hendon H. 2004. An all-season real-time multivariate MJO index: development of an index for monitoring and prediction. *Mon. Weather Rev.* **132**: 1917–1932.
- Widlansky MJ, Webster PJ, Hoyos CD. 2011. On the location and orientation of the South Pacific convergence zone. *Clim. Dyn.* **36**: 561–578.
- Wilks DS. 2011. *Statistical Methods in the Atmospheric Sciences*, Vol. **100**. 2nd edition. Academic Press: Amsterdam, 627.
- Yeh SW, Kug JS, Dewitte B, Kwon MH, Kirtman BP, Jin FF. 2009. El Niño in a changing climate. *Nature* **461**(7263): 511–514.
- Yiou P, Nogaj M. 2004. Extreme climatic events and weather regimes over the North Atlantic: when and where? *Geophys. Res. Lett.* **31**(7): L07202. <https://doi.org/10.1029/2003GL019119>.